Ammonium Fluoride Mediated Synthesis of Anhydrous Metal Fluoride−Mesoporous Carbon Nanocomposites for High-Performance Lithium Ion Battery Cathodes

Jinyoung Chun,[†] Changshin Jo,[†] Sunhye Sahgong,[∥] Min Gyu Kim,[‡] Eunho Lim,[§] Dong Hyeon Kim,[∥] Jongkook Hwang,[†] Eunae Kang,[†] Keun Ah Ryu,[†] Yoon Seok Jung,[∥] Youngsik Kim,[*,∥] and Jinwoo Lee[*,†,§]

[†]Department of Chemical Engineering, [‡]Beamline Research Division, Pohang Accelerator Laboratory, and [§]School of Environmental Science and Engineering, Pohang University of Science and Technology (POSTECH), Pohang 790-784, Republic of Korea
[∥]School of Energy and Chemical Engineering, Ulsan National Institute of Science and Technology (UNIST), Ulsan 689-798, Republic of Korea

Ⓢ Supporting Information

ABSTRACT: Metal fluorides (MF_x) are one of the most attractive cathode candidates for Li ion batteries (LIBs) due to their high conversion potentials with large capacities. However, only a limited number of synthetic methods, generally involving highly toxic or inaccessible reagents, currently exist, which has made it difficult to produce well-designed nanostructures suitable for cathodes; consequently, harnessing their potential cathodic properties has been a challenge. Herein, we report a new bottom-up synthetic method utilizing ammonium fluoride (NH_4F) for the preparation of anhydrous MF_x (CuF_2, FeF_3, and CoF_2)/mesoporous carbon (MSU−F−C) nanocomposites, whereby a series of metal precursor nanoparticles preconfined in mesoporous carbon were readily converted to anhydrous MF_x through simple heat treatment with NH_4F under solventless conditions. We demonstrate the versatility, lower toxicity, and efficiency of this synthetic method and, using XRD analysis, propose a mechanism for the reaction. All MF_x/MSU−F−C prepared in this study exhibited superior electrochemical performances, through conversion reactions, as the cathode for LIBs. In particular, FeF_3/MSU−F−C maintained a capacity of 650 mAh g^{-1}_{FeF3} across 50 cycles, which is ∼90% of its initial capacity. We expect that this facile synthesis method will trigger further research into the development of various nanostructured MF_x for use in energy storage and other applications.

KEYWORDS: metal fluorides, ammonium fluoride, lithium ion batteries, nanocomposites, high-capacity cathodes
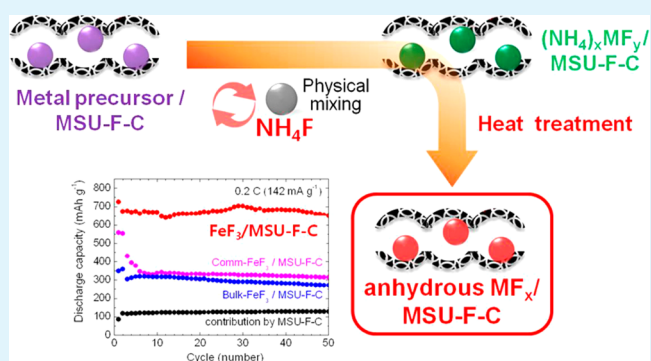
1. INTRODUCTION

The development of high-capacity electrode materials for Li ion batteries (LIBs) is essential to meeting the increased energy consumption of portable devices, the rapid growth of electrical vehicles, and the demand for advanced energy storage systems.[1,2] To replace the existing Li ion intercalation materials that have intrinsic capacity limitations, many researchers have focused on new electrode materials reacting through conversion or alloying reactions, which are able to take up multiple Li ions per unit formula.[3,4] Various materials, such as metal oxides,[5−7] metal sulfides,[8−10] metal nitrides,[8,11,12] and group 14 elements (Si, Ge, and Sn),[13−18] have been studied repeatedly in recent years. However, because the average operating voltages of these materials are generally low (vs Li/Li$^+$), most studies concentrated on anode materials. Therefore, exploitation of new conversion or alloying reaction-based cathode materials that exhibit high operating voltage with large capacity is one of the most urgent challenges we face today.

Among various metal compounds, metal fluorides (MF_x) are promising cathode candidates for LIBs as they exhibit high operating voltages as well as large specific capacities (Figure 1).[3,19] The high ionicity of the metal−fluoride (M−F) bond results in it displaying higher reaction potentials than other metal compounds, with two to three Li ions per formula unit participating in the electrochemical processes through conversion reactions.[20−22] Specifically, CuF_2 has the highest theoretical voltage (3.55 V vs Li/Li$^+$) among binary MF_x as well as a large specific capacity (528 mAh g^{-1}; $CuF_2 + 2 Li^+ + 2 e^- \leftrightarrow Cu + 2 LiF$). FeF_3 has one of the largest theoretical energy densities (1951 Wh kg^{-1}; $FeF_3 + xLi^+ + xe^- \leftrightarrow Li_xFeF_3$ // $Li_xFeF_3 + 3−x Li^+ + 3−x e^- \leftrightarrow Fe + 3 LiF$) among the MF_x family. Some different kinds of metal fluorides, such as CoF_2, also have large specific capacities (>500 mAh g^{-1}; $CoF_2 + 2 Li^+$

Figure 1. Voltage vs capacity of main intercalation materials and metal compounds. The represented points for metal fluorides,[23] metal sulfides,[23] metal nitrides,[24] metal oxides,[23,24] alloying materials,[13] and main intercalation materials[2] are based on theoretical capacities and average operating voltages (Adapted from refs 2 and 24 with permission from Royal Society of Chemistry and refs 13 and 23 with permission from Elsevier).

$+ 2 \text{ e}^- \leftrightarrow \text{Co} + 2 \text{ LiF}$) with high theoretical operating voltages (>2.5 V vs Li/Li$^+$).[23]

However, the low electronic conductivity and poor kinetics of the conversion reactions are critical shortcomings of MF$_x$ as cathodes for LIBs.[3,24] Thus, the nanostructuring of MF$_x$ with conducting materials is considered a prerequisite for their application.[20,25] However, compared to other metal compounds, there are few established methods for preparing MF$_x$ nanocomposites. For example, in the case of CuF$_2$, only top-

down approaches (e.g., ball milling of bulk materials) have been reported for the preparation of nanocomposites;[26−30] this method can neither control the morphology of the particles nor fabricate designed nanostructures.[31] CoF$_2$ could be obtained via synthetic methods other than the aforementioned top-down approach; however, established coprecipitation or supercritical fluid method resulted primarily in aggregated or large-sized CoF$_2$ nanoparticles.[32−34] Although many studies related to FeF$_3$ have been reported,[35−48] highly toxic materials,[35−40] expensive precursors,[41−46] and complicated processes[47,48] were required for its synthesis, and the obtained nanostructures were also limited. Moreover, MF$_x$ could be easily defluorinated during the heat treatment process for post carbon coating; which may be one of the main obstacles for preparing MF$_x$ electrodes. For these reasons, the synthesis of MF$_x$ nanocomposites suitable for use as cathodes for LIBs has been difficult over the past several decades. Consequently, most studies have focused on a limited material (FeF$_3$) within the range of intercalation reactions,[35,40,44−49] and inferior electrochemical performances were inevitable when conversion reactions progressed.[36,38,39,50] Few reports have evaluated CuF$_2$ and CoF$_2$ for LIBs and have presented only the first discharging step at very slow current rates[26−29] or have shown that the capacity decreases abruptly in subsequent cycles.[30,32−34] In this sense, to fully utilize the advantages of MF$_x$ cathode materials, a facile and general synthetic method for various anhydrous MF$_x$ needs to be developed; furthermore, the resulting MF$_x$ must exhibit not only high capacities based on conversion reactions but also stable cycling properties.

Figure 2. (a) Synthetic procedures for MF$_x$−mesoporous carbon nanocomposites (MF$_x$/MSU−F−C). (b) XRD patterns of CuF$_2$/MSU−F−C and bulk−CuF$_2$. (c) XRD patterns of FeF$_3$/MSU−F−C and bulk FeF$_3$. Asterisks indicate peaks from (NH$_4$)$_{0.18}$FeF$_3$. (d) XRD patterns of CoF$_2$/MSU−F−C and bulk−CoF$_2$. Asterisk indicates a peak from Co$_3$O$_4$. MF$_x$ synthesized using only metal precursors and NH$_4$F (without MSU−F−C) are designated as bulk−MF$_x$. Information about standard patterns of copper compounds was obtained from CuF$_2$ (JCPDS no. 81-0486), FeF$_3$ (JCPDS no. 88-2023), and CoF$_2$ (JCPDS no. 81-2033).

In this study, to address these critical issues and realize potential cathodic performance of MF_x in LIBs, we have developed a new bottom-up approach using ammonium fluoride (NH_4F) to synthesize anhydrous MF_x(CuF_2, FeF_3, and CoF_2)/mesoporous carbon($MSU-F-C$) nanocomposites. We discovered that various metal precursor nanoparticles preconfined in mesoporous carbon can be directly converted to anhydrous MF_x by simple heat treatment with NH_4F under solventless conditions. XRD analysis showed that, upon reaction with NH_4F, metal precursors were converted to the corresponding ammonium metal fluorides, $(NH_4)_xMF_y$, followed by decomposition to the desired anhydrous MF_x during further heat treatment. In this approach, the versatility of the synthetic method, mild toxicity of the process, and negligible product loss are considered distinctive advantages. Furthermore, when employed as the cathodes of LIBs, these well-dispersed MF_x nanoparticles in $MSU-F-C$ exhibited not only large discharge capacities through conversion reactions but also superior cycle performances and rate capabilities, all of which are electrochemical properties that have not been seen previously in these materials. Especially, FeF_3/$MSU-F-C$ maintained a capacity of 650 mAh g^{-1}_{FeF3} across 50 cycles, which is ~90% of its initial capacity. We expect that this facile synthetic method will initiate further research into the development of various nanostructured metal fluorides for use in energy storage and other applications.

2. RESULTS AND DISCUSSION

2.1. Synthesis of Metal Fluoride/Mesoporous Carbon Nanocomposites (MF_x/$MSU-F-C$). To confine nanosized active materials into the pores with high dispersibility and to provide an electron-conducting pathway, mesoporous carbon (mesocellular carbon foam, $MSU-F-C$)[51,52] was used as a support for the MF_x. The procedure developed for MF_x/$MSU-F-C$ synthesis is depicted in Figure 2a. The metal precursors were incorporated into the pores of $MSU-F-C$ by impregnation of the ethanolic metal nitrate solution. The precursor solution was easily diffused into the pores of $MSU-F-C$ by capillary forces. The target MF_x loading was 55 wt %, and the number of moles of metal precursor used was equal to the desired number of moles of MF_x. After the evaporation of solvent followed by further drying at 80 °C (designated as metal precursor/$MSU-F-C$), the metal precursors were incorporated into the pores of $MSU-F-C$. The resultant materials were mechanically ground with excess NH_4F to ensure complete reaction between the metal precursors and NH_4F. This mixture was heated at 200−270 °C under an inert atmosphere to convert the metal precursors to the desired MF_x (detailed procedures are described in Methods). Analysis of the obtained X-ray diffraction (XRD) patterns (Figure 2b−d) shows the formation of the desired MF_x/$MSU-F-C$ nanocomposites containing CuF_2, FeF_3, and CoF_2, whereby the collected diffraction patterns match the standard patterns of monoclinic CuF_2 (JCPDS no. 81-0486), rhombohedral FeF_3 (JCPDS no. 88-2023), and tetragonal CoF_2 (JCPDS no. 81-2033), respectively. A small and broad peak at around 25° due to the amorphous carbon supports indicates that metal precursors introduced into the $MSU-F-C$ were well-converted to their MF_x counterparts during heat treatment with NH_4F.

The loading of MF_x into the $MSU-F-C$ was further confirmed by various analytical techniques. As shown in the scanning electron microscopy (SEM) and transmission electron

microscopy (TEM) images (Figure 3a), $MSU-F-C$ has uniform mesocellular pores with diameters in the 30−40 nm
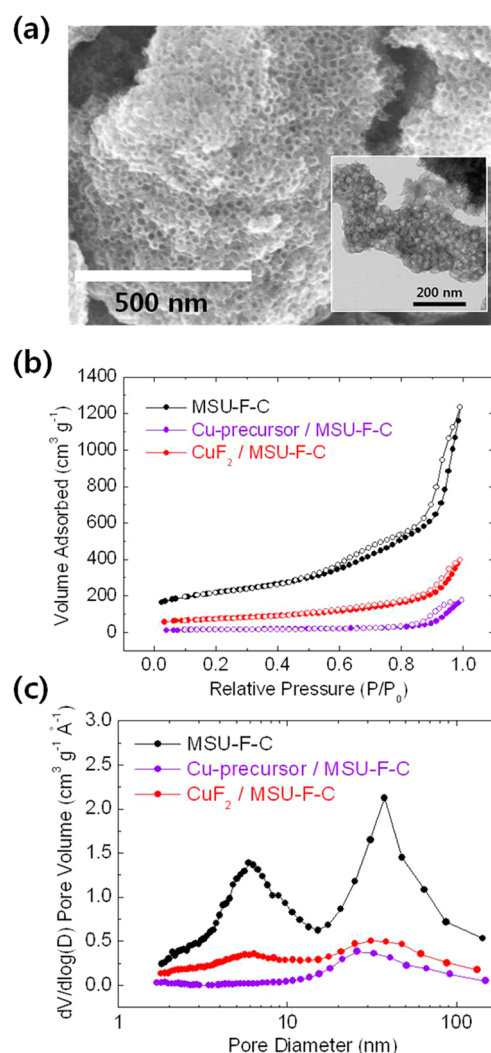

Figure 3. (a) SEM and TEM (inset) images of $MSU-F-C$. (b) N$_2$ physisorption isotherms and (c) pore-size distribution of $MSU-F-C$, Cu precursor/$MSU-F-C$, and CuF_2/$MSU-F-C$.

range. Nitrogen (N$_2$) physisorption isotherms (Figure 3b) and pore-size distribution (Figure 3c) indicate the existence of two kinds of mesopores: ~5 nm sized mesopores generated by the dissolution of the template walls and 30−40 nm sized mesopores originating from the main pores of the template,[51,52] having a large surface area (~800 m^2 g^{-1}) and pore volume (1.9 cm^3 g^{-1}). These pore structures and surface properties enable the loading nanoparticles larger than 10 nm into the pores without severe aggregation and provide extensive interconnected electron pathways.[53] Upon inclusion of the MF_x into $MSU-F-C$, the presence of the nanoparticles could be clearly observed, and the overall morphology of $MSU-F-C$ was not changed significantly. In the case of CuF_2, SEM images (Figure 4a,b) show that most of the CuF_2 nanoparticles were located in the pores of $MSU-F-C$, and a portion of these nanoparticles became overgrown and protruded from the $MSU-F-C$ pores (Figure 4b). Bulk-sized CuF_2 particles (bulk−CuF_2, Figure S1a,b) synthesized using only Cu precursors and NH_4F, without impregnation in $MSU-F-C$, are not observed. The morphologies of CuF_2/$MSU-F-C$ were
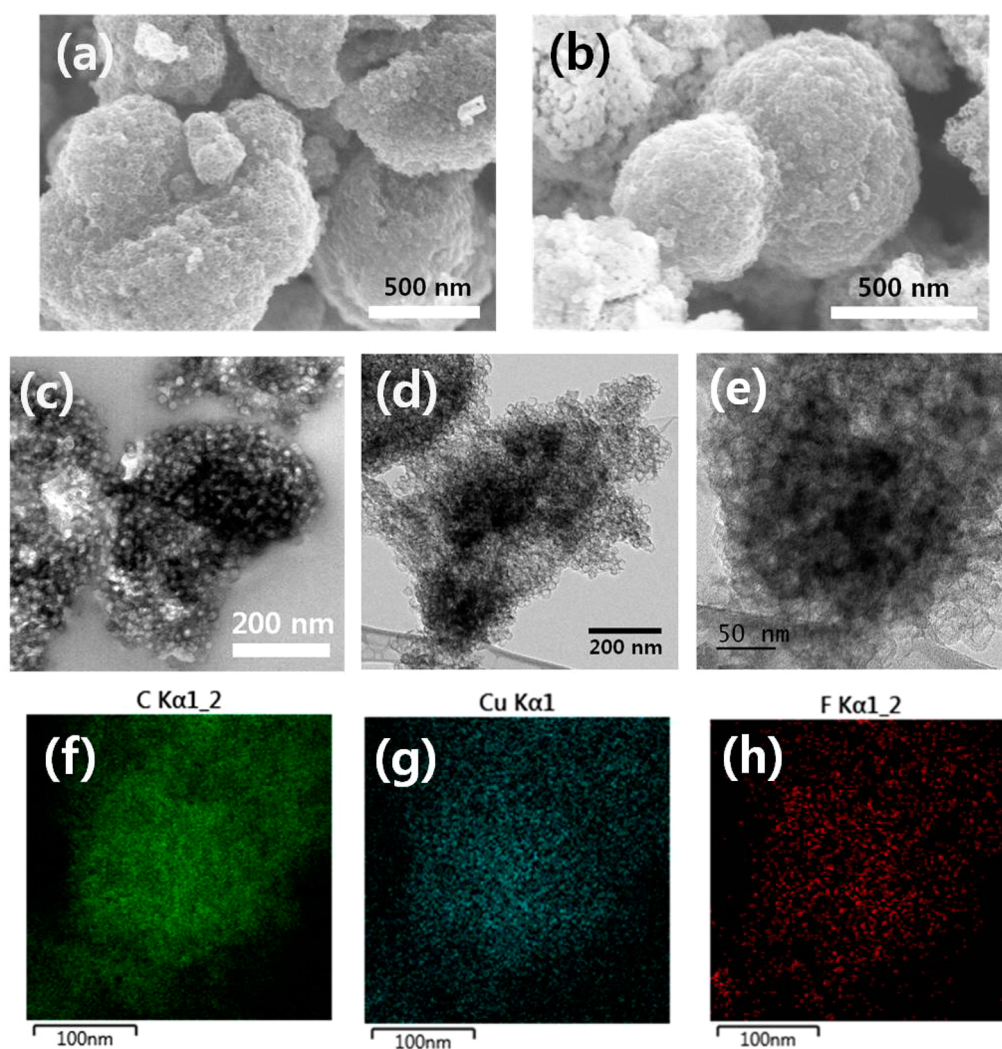
Figure 4. (a,b) SEM images of CuF$_2$/MSU−F−C. (c) TEM image of microtomed CuF$_2$/MSU−F−C. (d,e) TEM images of CuF$_2$/MSU−F−C. (f) Carbon, (g) copper, and (h) fluorine mapping corresponding to a TEM image shown in panel e.

also confirmed by TEM (Figure 4c−e). Elemental mapping results corresponding to TEM images demonstrate the existence of CuF$_2$ nanoparticles (Figures 4f−h and S2). As shown in TEM images, CuF$_2$ particles were loaded in the form of tiny dispersed nanoparticles or over 10 nm-sized particles (Figure S2 and section S2 in the Supporting Information). Similar features were also observed in the SEM and TEM images of FeF$_3$/MSU−F−C and CoF$_2$/MSU−F−C (Figures S3 and S4). Analysis of the N$_2$ physisorption isotherms provides further evidence of MF$_x$ loading in the MSU−F−C, whereby the surface areas and pore volumes of MF$_x$/MSU−F−C not only decreased significantly compared to those of MSU−F−C but also were smaller than those of simple mixtures of bulk−MF$_x$ and MSU−F−C (Table S1); these results indicate that the MF$_x$ nanoparticles grew inside the pores, which affected the surface properties of MSU−F−C. The pore-size distributions shown in Figure 3c (CuF$_2$) and Figure S5b,d (FeF$_3$ and CoF$_2$) also show the facile infiltration of the metal precursor and growth of the various MF$_x$ nanoparticles in the pores of MSU−F−C. Because small-sized pores are preferentially filled with precursor solution during the impregnation step by strong capillary forces, the pore volume of the small pores is expected to decrease much more than that of the large pores in MSU−F−C. A monomodal-shaped curve of metal

precursor/MSU−F−C with a peak at 30−40 nm coincides with this expectation. After heat treatment with NH$_4$F, precursor decomposition and subsequent particle growth led to re-exposure of the small-sized pores, and thus a bimodal-shaped curve with reduced peak intensity is observed.

2.2. Ammonium Fluoride Mediated Synthesis of MF$_x$. The main strategy of this synthetic method involves the reaction of metal precursors with decomposition products of NH$_4$F under solventless conditions (Figure 5a). NH$_4$F sublimes at 100 °C and decomposes to ammonia and hydrogen fluoride. Therefore, we expected that some anhydrous fluoride compounds could be obtained from reactions with decomposition products of NH$_4$F under an inert atmosphere. After the formation of fluoride compounds, the absence of ions or molecules (e.g., −OH and H$_2$O), which could result in unwanted defluorination at the reaction temperature (>100 °C), is considered the crucial factor for successful synthesis of anhydrous MF$_x$ in this method. The XRD patterns in Figure 5b−d present the changes in the crystalline phase during heat treatment with NH$_4$F, and these results support our prediction. Specifically, metal precursors converted to ammonium metal fluorides, (NH$_4$)$_x$MF$_y$, through reaction with decomposition products of NH$_4$F at 100 °C. (NH$_4$)$_x$MF$_y$ slowly decomposed to NH$_4$MF$_{x+1}$ during the intermediate stage, and further heat
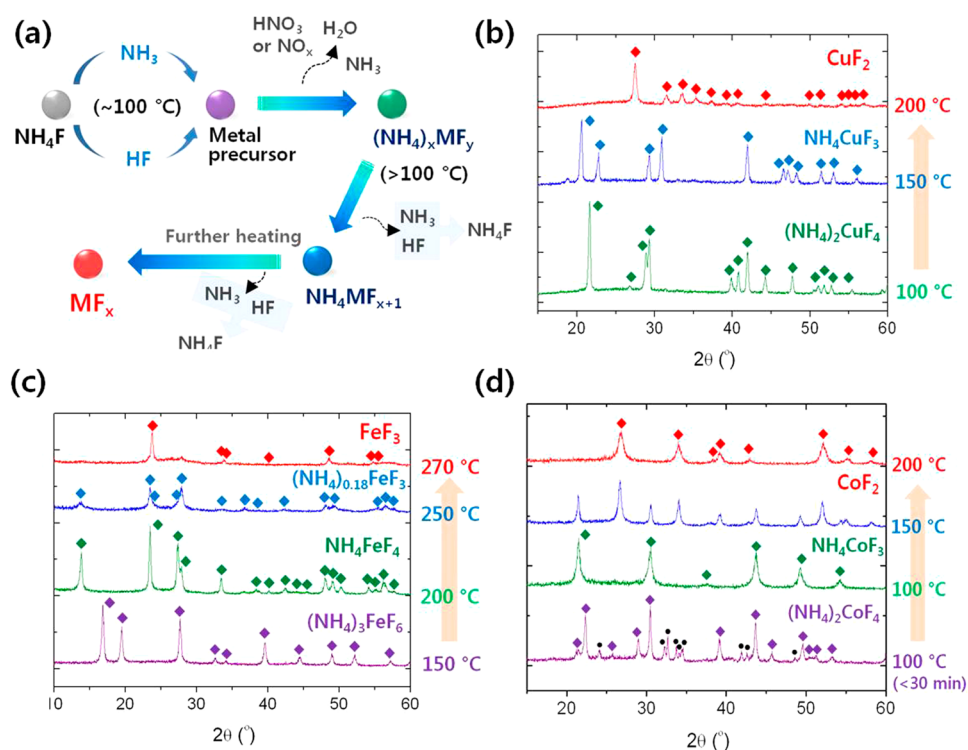
Figure 5. (a) Reaction mechanism of NH_4F-mediated synthesis of MF_x. (b−d) Crystalline phase change of (b) CuF_2/MSU−F−C, (c) FeF_3/MSU−F−C, and (d) CoF_2/MSU−F−C during heat treatment with NH_4F. Information about standard patterns of compounds was obtained from $(NH_4)_2CuF_4$ (JCPDS no. 49-0103), NH_4CuF_3 (JCPDS no. 77-0955), $(NH_4)_3FeF_6$ (JCPDS no. 22-1040), NH_4FeF_4 (JCPDS no. 20-0094), $(NH_4)_{0.18}FeF_3$ (JCPDS no. 47-0646), $(NH_4)_2CoF_4$ (JCPDS no. 18-0132), and NH_4CoF_3 (JCPDS no. 21-0699). Black dots in panel d indicate peaks from NH_4HF_2.
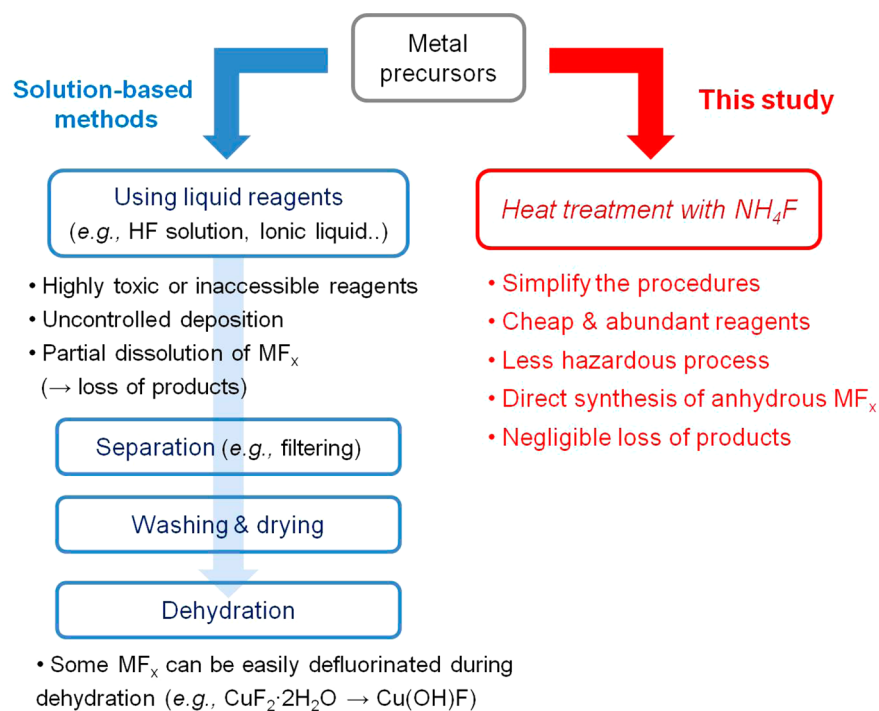
Figure 6. Advantages of NH_4F-mediated synthesis method (this study) and a comparison with general solution-based methods.

treatment led to the formation of anhydrous MF_x. From the reaction mechanism proposed, we also found that various metal compounds, which are converted to $(NH_4)_xMF_y$ without side products, could be used as precursors for the synthesis of anhydrous MF_x (Figure S6 and section S5 in the Supporting Information).

In addition to being versatile, this synthesis approach to preparing MF_x has several further advantages to the methods reported previously (Figure 6). First of all, compared to
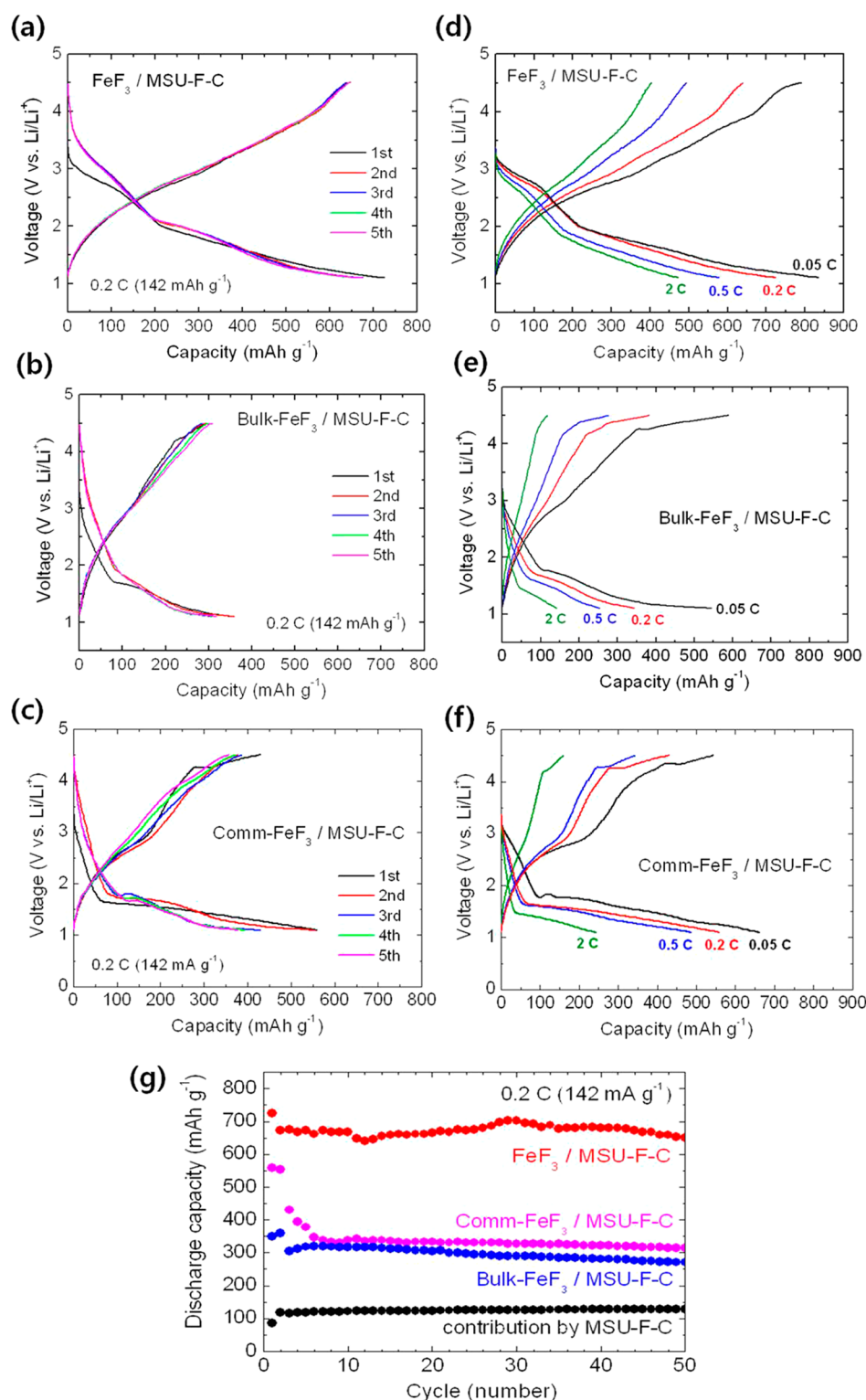
Figure 7. (a−c) Voltage profiles of (a) FeF$_3$/MSU−F−C nanocomposites, (b) bulk−FeF$_3$/MSU−F−C mixture, and (c) comm−FeF$_3$/MSU−F−C mixture at 0.2 C. (d−f) Voltage profiles of (d) FeF$_3$/MSU−F−C nanocomposite, (e) bulk−FeF$_3$/MSU−F−C mixture, and (f) comm−FeF$_3$/MSU−F−C mixture at the first cycle with various current densities. (g) Cycle properties of FeF$_3$/MSU−F−C nanocomposites, bulk−FeF$_3$/MSU−F−C mixture, and comm−FeF$_3$/MSU−F−C mixture at 0.2 C. Black dots indicate discharge capacities originating from MSU−F−C.

established methods, the procedure is very simple and relatively safe. Although the generation of small amount of toxic byproducts is possible and unavoidable, highly toxic compounds (e.g., fluorine gas or HF solution) are not required as a reactant (further discussion on the safety of the synthetic method is discussed in Figure S7 section S6 in the Supporting Information). Second, the direct synthesis of moisture sensitive and easily defluorinated MF$_x$, such as CuF$_2$, avoids the formation of undesirable hydration products (Figure S8). Lastly, because the reactions progresses under solventless
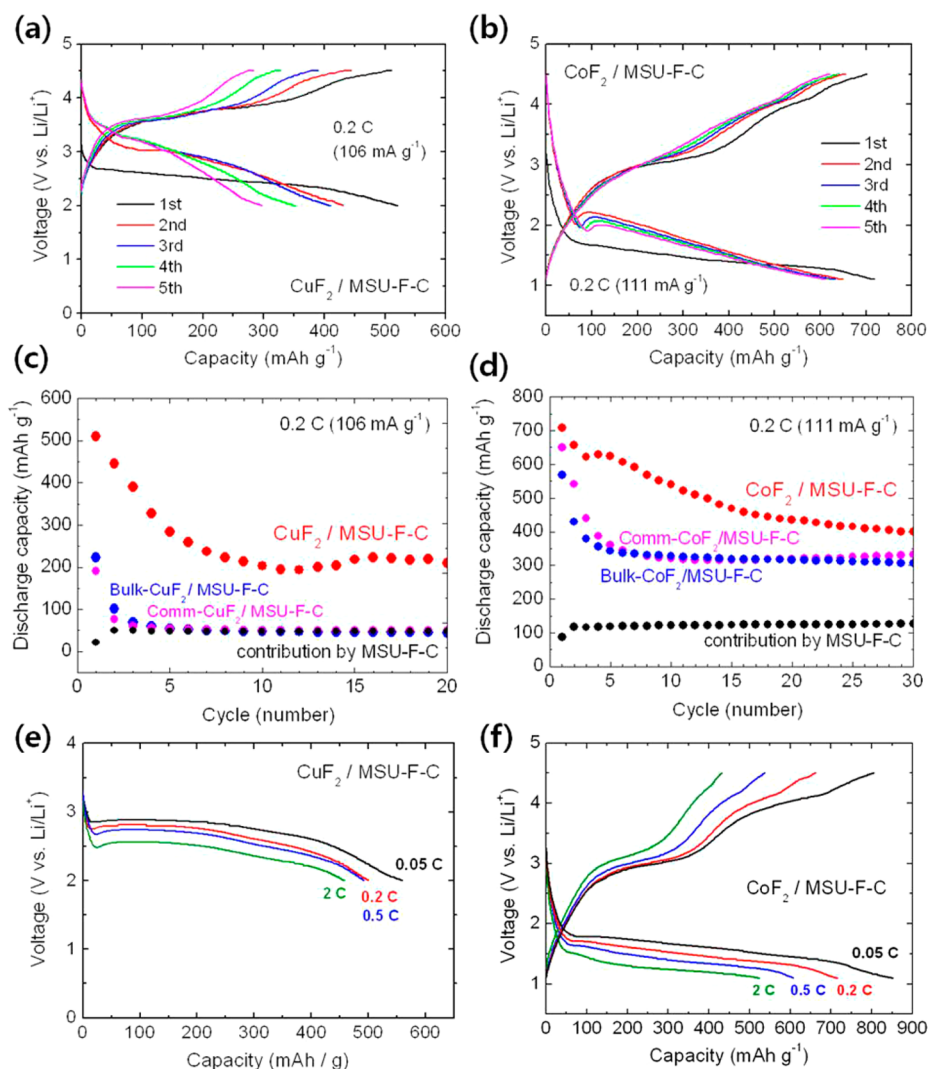
Figure 8. (a,b) Voltage profiles of (a) CuF$_2$/MSU−F−C and (b) CoF$_2$/MSU−F−C nanocomposites at 0.2 C. (c,d) Cycle properties of (c) CuF$_2$/MSU−F−C nanocomposites, bulk−CuF$_2$/MSU−F−C mixture, and comm−CuF$_2$/MSU−F−C mixture, and (d) CoF$_2$/MSU−F−C nanocomposites, bulk−CoF$_2$/MSU−F−C mixture, and comm−CoF$_2$/MSU−F−C mixture at 0.2 C. Black dots indicate discharge capacities originating from MSU−F−C. (e,f) Voltage profiles of (e) CuF$_2$/MSU−F−C nanocomposites at the first discharge and (f) CoF$_2$/MSU−F−C nanocomposites at the first cycle with various current densities. The rechargeability of CuF$_2$/MSU−F−C was tested using a solid-electrolyte-incorporated cell, whereas other results were obtained using normal coin-type cells.

conditions, the loss of products and subsequent decreases in yield through the partial dissolution of fluoride compounds is prevented; thermogravimetric analysis (TGA) results show that the MF$_x$ contents in the MF$_x$/MSU−F−C nanocomposites (55 wt %) were almost consistent with the target value (Figure S9).

2.3. Electrochemical Properties of MF$_x$/MSU−F−C. The electrochemical properties of MF$_x$/MSU−F−C nanocomposites as the cathodes of LIBs were evaluated by galvanostatic measurements. Focusing on the properties of MF$_x$, the specific capacities and current rates were calculated based on the mass of MF$_x$ (55 wt %). Among three kinds of MF$_x$/MSU−F−C, Figure 7 shows the results of electrochemical measurements of FeF$_3$/MSU−F−C first. Voltage profiles of FeF$_3$/MSU−F−C in Figure 7a present the characteristics of FeF$_3$, where an abrupt change in profile around 2.0 V indicates the progress of intercalation reaction (above 2.0 V) followed by conversion reactions (below 2.0 V).[54] The discharge capacity at the first cycle was 724 mAh g$^{-1}_{FeF3}$, and, even when the capacity contribution by MSU−F−C (~85 mAh g^{-1} at the first

discharge; Figure S10) is excluded, almost 640 mAh g$^{-1}_{FeF3}$ of capacity originated from FeF$_3$ component of the nanocomposites (theoretical capacity of FeF$_3$: 712 mAh g^{-1}). In contrast, the specific capacities of bulk-FeF$_3$/MSU−F−C, which is a physical mixture of bulk−FeF$_3$ (Figure S1c,d) and MSU−F−C, were significantly lower than those of its nanocomposites analog (Figure 7b), and a physical mixture of commercial FeF$_3$ and MSU−F−C (designated as comm−FeF$_3$/MSU−F−C) also showed low specific capacities compared to FeF$_3$/MSU−F−C (Figure 7c). More impressively, FeF$_3$/MSU−F−C maintained a capacity of 650 mAh g$^{-1}_{FeF3}$ across 50 cycles (Figure 7g), which is ~90% of its initial capacity, such that, even if the mass of all of the active materials (FeF$_3$ and MSU−F−C) is considered, more than 350 mAh g$^{-1}_{total}$ of capacity was maintained over 50 cycles. This result indicates that FeF$_3$/MSU−F−C exhibited excellent cycle performance, even as the conversion reactions progressed (Table S2 compares the electrochemical performance of FeF$_3$ in the representative papers).[36,38,39,42,50,54−56] It is considered

that gradual increase of capacity up to 30th cycle and decrease of capacity in the following cycles originated from the combination of positive electrode activation and stabilization effect[57−59] and negative electrode degradation[36,60] (e.g., irreversible conversion reaction or other side reactions). Similar phenomenon was also observed in the previous papers, in which iron oxyfluoride[61] or iron−LiF nanocomposites[62,63] were studied as conversion reaction-based cathodes for LIBs. FeF$_3$/MSU−F−C also exhibited good rate capability (Figure 7d), where, even at a high current rate of 2 C, more than 470 mAh g$^{-1}_{FeF3}$ of capacity was retained, this value corresponding to ~57% of capacity at 0.05 C. Although bulk−FeF$_3$/MSU−F−C and comm−FeF$_3$/MSU−F−C showed relatively high discharge capacity (544 mAh g$^{-1}_{FeF3}$ and 662 mAh g$^{-1}_{FeF3}$, respectively) at a very slow current rate (0.05 C), abrupt decreases in capacity were observed at high current rates (panels e and f of Figure 7, respectively).

Voltage profiles of CuF$_2$/MSU−F−C and CoF$_2$/MSU−F−C at 0.2 C are shown in panels a and b of Figure 8, respectively. CuF$_2$/MSU−F−C began to react with Li ions at slightly below 3.0 V, while CoF$_2$/MSU−F−C reacted at around 1.5 V; each electrode presented characteristics of CuF$_2$ and CoF$_2$.[26,32] Excluding the contribution by MSU−F−C (Figure S10b), CuF$_2$/MSU−F−C exhibited 489 mAh g$^{-1}_{CuF2}$ of discharge capacity at the first cycle, a value that is close to the theoretical capacity of CuF$_2$ (528 mAh g^{-1}). CoF$_2$/MSU−F−C also showed superior discharge capacity at the first cycle (623 mAh g$^{-1}_{CoF2}$, excluding contribution by MSU−F−C in Figure S9a), which is larger than the theoretical capacity of CoF$_2$ (553 mAh g^{-1}); it is inferred that additional capacity observed originates from interfacial Li storage by CoF$_2$ at low voltages.[33] Meanwhile, in contrast to FeF$_3$/MSU−F−C, discharge capacities of CuF$_2$/MSU−F−C and CoF$_2$/MSU−F−C decreased rapidly during subsequent cycles (panels c and d of Figure 8), degradation that is proposed to be a result of dissolution of the metals in the active materials at high voltages (Figure S11 and section S10 of the Supporting Information). In the case of CuF$_2$/MSU−F−C, cell failure occurred during the first charging step when a normal coin-type cell was employed (Figure S11d), so to overcome this problem, recharging was tested using a solid-electrolyte-incorporated cell (Figure S12). In both of the nanocomposites, a decrease in capacity was observed, however: 209 mAh g$^{-1}_{CuF2}$ (at the 20th cycle) and 400 mAh g$^{-1}_{CoF2}$ (at the 30th cycle) of discharge capacities were retained in the CuF$_2$/MSU−F−C and CoF$_2$/MSU−F−C cells, respectively. These results show improved performance in comparison to previous studies;[26−28,30,32−34] in particular, this is the first result that shows promising cycle properties of CuF$_2$.

Panels e and f of Figure 8 present rate capability of CuF$_2$/MSU−F−C and CoF$_2$/MSU−F−C, respectively. To eliminate large polarization by internal resistances of the solid-electrolyte-incorporated cell as well as cell failure, the rate properties of CuF$_2$/MSU−F−C were tested using a normal coin-type cell at the first discharging step only. In the case of CuF$_2$/MSU−F−C, even at a high current rate of 2 C, almost 80% of the discharge capacity at 0.05 C was retained (455 mAh g$^{-1}_{CuF2}$). CoF$_2$/MSU−F−C also exhibited 523 mAh g$^{-1}_{CoF2}$ of discharge capacity at 2 C, which corresponds to ~62% of discharge capacity at 0.05 C. Similar to that observed for FeF$_3$/MSU−F−C, both CuF$_2$/MSU−F−C and CoF$_2$/MSU−F−C presented excellent rate capability. In contrast, bulk−MF$_x$ (CuF$_2$ or CoF$_2$)/MSU−F−C and comm−MF$_x$ (CuF$_2$ or CoF$_2$)/MSU−F−C showed poor performance in its discharge capacity and

rate capability (Figures S13 and S14, respectively). Interestingly, the specific capacities of bulk−CoF$_2$/MSU−F−C and comm−CoF$_2$/MSU−F−C at low current rates were relatively large (Figures S13d and S14d, respectively), which we propose is a result of the small size of the bulk−CoF$_2$ and comm−CoF$_2$ particles in comparison to other bulk−MF$_x$ particles (Figures S1 and S15, respectively), thereby allowing the conversion reactions to progress actively at low current rates.

The electrochemical results presented in the Figure 7 and 8 reveal the superior performances of the MF$_x$/MSU−F−C nanocomposites. It is proposed that these well-dispersed MF$_x$ nanoparticles within a mesoporous conducting matrix led to facile conversion reactions because of (i) the effective electron transport, (ii) the short diffusion length of Li ions, and (iii) the relatively fast kinetics of well-dispersed nanoparticles.[64−67] These results are of high significance in the potential application of MF$_x$ as high-capacity cathodic materials in LIBs, as the limitation of MF$_x$ that have been identified in previous studies are overcome. However, for the practical use of MF$_x$ as a cathode, further improvement to electrochemical performance and elucidation of the reaction mechanism are required. First, rational electrode design or electrolyte development for effective prevention of active material dissolution is necessary to improve cycle properties.[68−70] Increasing the ratio of active materials (MF$_x$) in the electrode without sacrificing performance is also an important issue.[14,58,71] In addition, in-depth research into conversion reactions of MF$_x$ should be accompanied by various in situ and ex situ analyses.[17,72] These issues will be addressed in a forthcoming paper.

3. CONCLUSIONS

In summary, we report a new bottom-up approach to the synthesis of anhydrous metal fluoride/mesoporous carbon (MF$_x$/MSU−F−C) nanocomposites using NH$_4$F, and, furthermore, we demonstrate their superior electrochemical performance when used as the cathodes of LIBs. We found that various MF$_x$ could be obtained from the metal compounds dispersed in MSU−F−C using a method of simple heat treatment under solventless conditions. This relatively facile, safe, and versatile method enabled the synthesis of various MF$_x$(CuF$_2$, FeF$_3$, and CoF$_2$)/MSU−F−C nanocomposites. As the cathodes of LIBs, these well-dispersed MF$_x$ nanoparticles in MSU−F-C exhibited superior electrochemical performance even as the conversion reactions progressed. FeF$_3$/MSU−F−C maintained a capacity of 650 mAh g$^{-1}_{FeF3}$ across 50 cycles, and CuF$_2$/MSU−F−C and CoF$_2$/MSU−F−C also retained 209 mAh g$^{-1}_{CuF2}$ (at the 20th cycle) and 400 mAh g$^{-1}_{CoF2}$ (at the 30th cycle) of capacities, respectively, all of which were improved cycle properties that have not been seen previously in these materials.

4. EXPERIMENTAL SECTION

4.1. Synthesis of MF$_x$/Mesoporous Carbon Nanocomposites (MF$_x$/MSU−F−C). Mesoporous carbon (mesocellular carbon foam, MSU−F−C) was synthesized by a hard template method using mesocellular aluminosilicate foam and furfuryl alcohol as silica template and carbon precursor, respectively, following the previously reported procedures.[52] For the synthesis of MF$_x$/MSU−F−C, metal precursors were loaded on the MSU−F−C by a wet impregnation method first. The desired amount of metal nitrate dissolved ethanolic solution was impregnated into the MSU−F−C at room temperature. For example, to load 55 wt % CuF$_2$ on MSU−F−C (e.g., 0.12 g of CuF$_2$ plus 0.1 g of MSU−F−C), 0.28 g of Cu(NO$_3$)$_2$·2.5H$_2$O dissolved ethanolic solution was impregnated into 0.1 g of MSU−F−C. After the

evaporation of ethanol under stirring, they were further dried in vacuum oven at 80 °C. The resultant materials were mechanically ground with excess amount of NH₄F (more than two times higher than minimum amounts needed for conversion to CuF_2) in a fume hood. The mixture was heated at 210 °C during 1−3 h under argon atmosphere. FeF_3/MSU−F−C and CoF_2/MSU−F−C were synthesized by the same procedure except that final mixtures (metal precursor/MSU−F−C mixed with NH₄F) were heated at 270 and 250 °C during 1.5 h, respectively. For the complete conversion of metal precursors to MF_x, heat treatment with NH₄F progressed two or three times. After heat treatment, the obtained materials were kept in an argon-filled glovebox. Bulk−MF_x was synthesized by the same procedure except that MSU−F−C was not used. Bulk−MF_x/MSU−F−C mixtures were prepared by the physical mixing of bulk−MF_x and MSU−F−C in an argon-filled glovebox. Commercial CuF_2 (anhydrous, 99.5%), FeF_3 (anhydrous, 97% min), and CoF_2 (anhydrous, 98%) were obtained from Alfa Aesar. Commercial MF_x/MSU−F−C mixtures (designated as comm−MF_x/MSU−F-C) were also prepared by physical mixing of commercial MF_x and MSU−F−C in an argon-filled glovebox.

4.2. Materials Characterizations. Powder X-ray diffraction (XRD) patterns were obtained with a Rigaku D/max-2500 diffractometer using Cu Kα radiation (λ = 1.5418 Å) at a scanning rate of 6.00° min⁻¹. The morphology was investigated using a transmission electron microscope (TEM, Hitachi H-7600) and a scanning electron microscope (SEM, Hitachi S-4800). Other TEM images and elemental mapping results were obtained using a JEOL JEM-2010. Energy-dispersive X-ray spectroscopy (EDS) was performed on a JEOL JSM-7401F. The nitrogen physisorption isotherms were measured at 77 K using a Tristar II 3020 system (Micromeritics Instrument Corporation). The samples were degassed overnight at 80−150 °C before measurements. The surface area of the samples were calculated from the isotherms according to the Brunauer−Emmett−Teller (BET) method, and pore volumes were taken at a single point, P/P_o = 0.995. The pore-size distributions were obtained from the adsorption branch using the Barett−Joyner−Halenda (BJH) method. Thermogravimetric analysis (TGA) was performed using a STA7300 thermal analysis system (Hitachi) under air atmosphere with a heating rate of 5 °C min⁻¹.

4.3. Electrochemical Characterizations. To prepare the electrodes, the active materials (MF_x/MSU−F−C) were mixed with polyvinylidene difluoride (PVDF) binder and conducting carbon (Super P) to a ratio of 7:2:1 by weight using N-methyl-2-pyrrolidone (NMP). The resulting slurries were coated onto a carbon-coated aluminum foil (Wellcos Co., Korea) and then dried in a vacuum condition. The average mass loading of MF_x/MSU−F−C was 0.5 mg cm⁻². Electrodes made of bulk−MF_x/MSU−F−C or comm−MF_x/MSU−F−C mixture were prepared by the same procedure, and their average mass loading (bulk−MF_x/MSU−F−C or comm−MF_x/MSU−F−C mixture) was also 0.5 mg cm⁻². Coin-type cells (CR2032) and solid-electrolyte-incorporated cells were assembled in an argon-filled glovebox, in which Li foil was used as the reference and counter electrode, and 1.0 M $LiPF_6$ in ethylene carbonate/dimethyl carbonate (EC/DMC, 1:1 volume ratio, PANAX E-TEC Co., Korea) was used as the electrolyte. The fabrication method of solid-electrolyte-incorporated cells was described elsewhere.[73] In the case of this study, 1.0 M $LiPF_6$ in EC/DMC was used as an electrolyte in both anode and cathode parts, and nickel mesh was used as current collector in the cathode side. Using a WBCS-3000 battery cycler (WonATech Co., Korea), the galvanostatic charge−discharge analyses were conducted in the potential range of 1.1−4.5 V (FeF_3 and CoF_2) or 2.0−4.5 V (CuF_2) vs Li/Li⁺ at different current rates. The specific capacities and current rates were calculated based on the mass of MF_x. To characterize components of cell after measurements, cells were disassembled in an argon-filled glovebox, and the Li foils and separators were washed with dimethyl carbonate (DMC) several times.

■ ASSOCIATED CONTENT

ⓢ Supporting Information

The Supporting Information is available free of charge on the ACS Publications website at DOI: 10.1021/acsami.6b10641.

> Additional experimental details. Figures showing SEM and TEM images, XRD patterns, and TGA results of materials; N₂ physisorption isotherms and pore-size distribution of materials; configuration of the heat-treatment apparatus used in this study; voltage profiles of MSU−F−C; photographs of Li metal and separator; voltage profiles; and a schematic diagram and photograph of the experimental setup. Tables showing EDS analysis results, BET surface area and pore volume of materials, and electrochemical properties of various FeF_3 cathode materials. (PDF)

■ AUTHOR INFORMATION

Corresponding Authors

*E-mail (Y.K.): ykim@unist.ac.kr.
*E-mail (J.L.): jinwoo03@postech.ac.kr.

Author Contributions

The manuscript was written through contributions of all authors. All authors have given approval to the final version of the manuscript.

Notes

The authors declare no competing financial interest.

■ ACKNOWLEDGMENTS

■ REFERENCES

(1) Goodenough, J. B.; Kim, Y. Challenges for Rechargeable Li Batteries. *Chem. Mater.* **2010**, 22, 587−603.

(2) Wang, Y.; Li, H.; He, P.; Hosono, E.; Zhou, H. Nano Active Materials for Lithium-Ion Batteries. *Nanoscale* **2010**, 2, 1294−1305.

(3) Cabana, J.; Monconduit, L.; Larcher, D.; Palacin, M. R. Beyond Intercalation-Based Li-Ion Batteries: The State of the Art and Challenges of Electrode Materials Reacting Through Conversion Reactions. *Adv. Mater.* **2010**, 22, E170−E192.

(4) Croguennec, L.; Palacin, M. R. Recent Achievements on Inorganic Electrode Materials for Lithium-Ion Batteries. *J. Am. Chem. Soc.* **2015**, 137, 3140−3156.

(5) Reddy, M.; Subba Rao, G.; Chowdari, B. Metal Oxides and Oxysalts as Anode Materials for Li Ion Batteries. *Chem. Rev.* **2013**, 113, 5364−5457.

(6) Pol, V. G.; Li, Y.; Dogan, F.; Secor, E.; Thackeray, M. M.; Abraham, D. P. Pulsed Sonication for Alumina Coatings on High-Capacity Oxides: Performance in Lithium-Ion Cells. *J. Power Sources* **2014**, 258, 46−53.

(7) Zhang, L.; Wu, H. B.; Lou, X. W. D. Iron-Oxide-Based Advanced Anode Materials for Lithium-Ion Batteries. *Adv. Energy Mater.* **2014**, 4, 1300958.

(8) Ji, L.; Lin, Z.; Alcoutlabi, M.; Zhang, X. Recent Developments in Nanostructured Anode Materials for Rechargeable Lithium-Ion Batteries. *Energy Environ. Sci.* 2011, 4, 2682−2699.

(9) Xu, X.; Fan, Z.; Yu, X.; Ding, S.; Yu, D.; Lou, X. W. D. A Nanosheets-on-Channel Architecture Constructed from MoS_2 and CMK-3 for High-Capacity and Long-Cycle-Life Lithium Storage. *Adv. Energy Mater.* 2014, 4, 1400902.

(10) Britto, S.; Leskes, M.; Hua, X.; Hébert, C.-A.; Shin, H. S.; Clarke, S.; Borkiewicz, O.; Chapman, K. W.; Seshadri, R.; Cho, J.; Grey, C. P. Multiple Redox Modes in the Reversible Lithiation of High-Capacity, Peierls-Distorted Vanadium Sulfide. *J. Am. Chem. Soc.* 2015, 137, 8499−8508.

(11) Fu, Z.-W.; Wang, Y.; Yue, X.-L.; Zhao, S.-L.; Qin, Q.-Z. Electrochemical Reactions of Lithium with Transition Metal Nitride Electrodes. *J. Phys. Chem. B* 2004, 108, 2236−2244.

(12) Sun, Q.; Fu, Z.-W. Vanadium Nitride as a Novel Thin Film Anode Material for Rechargeable Lithium Batteries. *Electrochim. Acta* 2008, 54, 403−409.

(13) Wu, H.; Cui, Y. Designing Nanostructured Si Anodes for High Energy Lithium Ion Batteries. *Nano Today* 2012, 7, 414−429.

(14) Yuan, F.-W.; Tuan, H.-Y. Scalable Solution-Grown High-Germanium-Nanoparticle-Loading Graphene Nanocomposites as High-Performance Lithium-Ion Battery Electrodes: An Example of a Graphene-Based Platform toward Practical Full-Cell Applications. *Chem. Mater.* 2014, 26, 2172−2179.

(15) Eom, K.; Jung, J.; Lee, J. T.; Lair, V.; Joshi, T.; Lee, S. W.; Lin, Z.; Fuller, T. F. Improved Stability of Nano-Sn Electrode with High-Quality Nano-SEI Formation for Lithium Ion Battery. *Nano Energy* 2015, 12, 314−321.

(16) Hwang, J.; Woo, S. H.; Shim, J.; Jo, C.; Lee, K. T.; Lee, J. One-Pot Synthesis of Tin-Embedded Carbon/Silica Nanocomposites for Anode Materials in Lithium-Ion Batteries. *ACS Nano* 2013, 7, 1036−1044.

(17) Mai, L.; Tian, X.; Xu, X.; Chang, L.; Xu, L. Nanowire Electrodes for Electrochemical Energy Storage Devices. *Chem. Rev.* 2014, 114, 11828−11862.

(18) Yi, R.; Zai, J.; Dai, F.; Gordin, M. L.; Wang, D. Dual Conductive Network-Enabled Graphene/Si−C Composite Anode with High Areal Capacity for Lithium-Ion Batteries. *Nano Energy* 2014, 6, 211−218.

(19) Li, H.; Balaya, P.; Maier, J. Li-Storage via Heterogeneous Reaction in Selected Binary Metal Fluorides and Oxides. *J. Electrochem. Soc.* 2004, 151, A1878−A1885.

(20) Li, H.; Richter, G.; Maier, J. Reversible Formation and Decomposition of LiF Clusters Using Transition Metal Fluorides as Precursors and Their Application in Rechargeable Li Batteries. *Adv. Mater.* 2003, 15, 736−739.

(21) Aricò, A. S.; Bruce, P.; Scrosati, B.; Tarascon, J.-M.; Van Schalkwijk, W. Nanostructured Materials for Advanced Energy Conversion and Storage Devices. *Nat. Mater.* 2005, 4, 366−377.

(22) Palacín, M. R. Recent Advances in Rechargeable Battery Materials: A Chemist's Perspective. *Chem. Soc. Rev.* 2009, 38, 2565−2575.

(23) Amatucci, G. G.; Pereira, N. Fluoride Based Electrode Materials for Advanced Energy Storage Devices. *J. Fluorine Chem.* 2007, 128, 243−262.

(24) Klein, F.; Jache, B.; Bhide, A.; Adelhelm, P. Conversion Reactions for Sodium-Ion Batteries. *Phys. Chem. Chem. Phys.* 2013, 15, 15876−15887.

(25) Yamakawa, N.; Jiang, M.; Key, B.; Grey, C. P. Identifying the Local Structures Formed during Lithiation of the Conversion Material, Iron Fluoride, in a Li Ion Battery: A Solid-State NMR, X-ray Diffraction, and Pair Distribution Function Analysis Study. *J. Am. Chem. Soc.* 2009, 131, 10525−10536.

(26) Badway, F.; Mansour, A.; Pereira, N.; Al-Sharab, J.; Cosandey, F.; Plitz, I.; Amatucci, G. Structure and Electrochemistry of Copper Fluoride Nanocomposites Utilizing Mixed Conducting Matrices. *Chem. Mater.* 2007, 19, 4129−4141.

(27) Yamakawa, N.; Jiang, M.; Grey, C. P. Investigation of the Conversion Reaction Mechanisms for Binary Copper (II) Compounds

(28) Mansour, A.; Badway, F.; Yoon, W.-S.; Chung, K.; Amatucci, G. In Situ X-Ray Absorption Spectroscopic Investigation of the Electrochemical Conversion Reactions of CuF_2−MoO_3 Nanocomposite. *J. Solid State Chem.* 2010, 183, 3029−3038.

(29) Wang, F.; Robert, R.; Chernova, N. A.; Pereira, N.; Omenya, F.; Badway, F.; Hua, X.; Ruotolo, M.; Zhang, R.; Wu, L.; et al. Conversion Reaction Mechanisms in Lithium Ion Batteries: Study of the Binary Metal Fluoride Electrodes. *J. Am. Chem. Soc.* 2011, 133, 18828−18836.

(30) Hua, X.; Robert, R.; Du, L.-S.; Wiaderek, K. M.; Leskes, M.; Chapman, K. W.; Chupas, P. J.; Grey, C. P. Comprehensive Study of the CuF_2 Conversion Reaction Mechanism in a Lithium-Ion Battery. *J. Phys. Chem. C* 2014, 118, 15169−15184.

(31) Gu, W.; Magasinski, A.; Zdyrko, B.; Yushin, G. Metal Fluorides Nanoconfined in Carbon Nanopores as Reversible High Capacity Cathodes for Li and Li-Ion Rechargeable Batteries: FeF_2 as an Example. *Adv. Energy Mater.* 2015, 5, 1401148.

(32) Teng, Y. T.; Pramana, S. S.; Ding, J.; Wu, T.; Yazami, R. Investigation of the Conversion Mechanism of Nanosized CoF_2. *Electrochim. Acta* 2013, 107, 301−312.

(33) Tan, J.; Liu, L.; Guo, S.; Hu, H.; Yan, Z.; Zhou, Q.; Huang, Z.; Shu, H.; Yang, X.; Wang, X. The Electrochemical Performance and Mechanism of Cobalt (II) Fluoride as Anode Material for Lithium and Sodium Ion Batteries. *Electrochim. Acta* 2015, 168, 225−233.

(34) Armstrong, M. J.; Panneerselvam, A.; O'Regan, C.; Morris, M. A.; Holmes, J. D. Supercritical-Fluid Synthesis of FeF_2 and CoF_2 Li-Ion Conversion Materials. *J. Mater. Chem. A* 2013, 1, 10667−10676.

(35) Ma, D.-l.; Cao, Z.-y.; Wang, H.-g.; Huang, X.-l.; Wang, L.-m.; Zhang, X.-b. Three-Dimensionally Ordered Macroporous FeF_3 and Its In Situ Homogenous Polymerization Coating for High Energy and Power Density Lithium Ion Batteries. *Energy Environ. Sci.* 2012, 5, 8538−8542.

(36) Li, L.; Meng, F.; Jin, S. High-Capacity Lithium-Ion Battery Conversion Cathodes Based on Iron Fluoride Nanowires and Insights into the Conversion Mechanism. *Nano Lett.* 2012, 12, 6030−6037.

(37) Zhou, H.; Ruther, R. E.; Adcock, J.; Zhou, W.; Dai, S.; Nanda, J. Controlled Formation of Mixed Nanoscale Domains of High Capacity Fe_2O_3−FeF_3 Conversion Compounds by Direct Fluorination. *ACS Nano* 2015, 9, 2530−2539.

(38) Ma, R.; Wang, M.; Tao, P.; Wang, Y.; Cao, C.; Shan, G.; Yang, S.; Xi, L.; Chung, J. C.; Lu, Z. Fabrication of FeF_3 Nanocrystals Dispersed into a Porous Carbon Matrix as a High Performance Cathode Material for Lithium Ion Batteries. *J. Mater. Chem. A* 2013, 1, 15060−15067.

(39) Liu, L.; Guo, H.; Zhou, M.; Wei, Q.; Yang, Z.; Shu, H.; Yang, X.; Tan, J.; Yan, Z.; Wang, X. A Comparison among $FeF_3 \cdot 3H_2O$, $FeF_3 \cdot 0.33 H_2O$ and FeF_3 Cathode Materials for Lithium Ion Batteries: Structural, Electrochemical, and Mechanism Studies. *J. Power Sources* 2013, 238, 501−515.

(40) Tan, J.; Liu, L.; Hu, H.; Yang, Z.; Guo, H.; Wei, Q.; Yi, X.; Yan, Z.; Zhou, Q.; Huang, Z.; Shu, H.; Yang, X.; Wang, X. Iron Fluoride with Excellent Cycle Performance Synthesized by Solvothermal Method as Cathodes for Lithium Ion Batteries. *J. Power Sources* 2014, 251, 75−84.

(41) Lu, Y.; Wen, Z.; Rui, K.; Wu, X.; Cui, Y. Worm-Like Mesoporous Structured Iron-Based Fluoride: Facile Preparation and Application as Cathodes for Rechargeable Lithium Ion Batteries. *J. Power Sources* 2013, 244, 306−311.

(42) Lu, Y.; Wen, Z.; Jin, J.; Wu, X.; Rui, K. Size-Controlled Synthesis of Hierarchical Nanoporous Iron Based Fluorides and Their High Performances in Rechargeable Lithium Ion Batteries. *Chem. Commun.* 2014, 50, 6487−6490.

(43) Lu, Y.; Wen, Z.; Jin, J.; Rui, K.; Wu, X. Hierarchical Mesoporous Iron-Based Fluoride with Partially Hollow Structure: Facile Preparation and High Performance as Cathode Material for Rechargeable Lithium Ion Batteries. *Phys. Chem. Chem. Phys.* 2014, 16, 8556−8562.

(44) Li, C.; Gu, L.; Tsukimoto, S.; van Aken, P. A.; Maier, J. Low-Temperature Ionic-Liquid-Based Synthesis of Nanostructured Iron-

Based Fluoride Cathodes for Lithium Batteries. *Adv. Mater.* **2010**, *22*, 3650−3654.

(45) Li, C.; Gu, L.; Tong, J.; Tsukimoto, S.; Maier, J. A Mesoporous Iron-Based Fluoride Cathode of Tunnel Structure for Rechargeable Lithium Batteries. *Adv. Funct. Mater.* **2011**, *21*, 1391−1397.

(46) Li, C.; Yin, C.; Gu, L.; Dinnebier, R. E.; Mu, X.; van Aken, P. A.; Maier, J. An $FeF_3 \cdot 0.5 \, H_2O$ Polytype: A Microporous Framework Compound with Intersecting Tunnels for Li and Na Batteries. *J. Am. Chem. Soc.* **2013**, *135*, 11425−11428.

(47) Long, Z.; Hu, W.; Liu, L.; Qiu, G.; Qiao, W.; Guan, X.; Qiu, X. Mesoporous Iron Trifluoride Microspheres as Cathode Materials for Li-ion Batteries. *Electrochim. Acta* **2015**, *151*, 355−362.

(48) Zhao, T.; Li, L.; Chen, R.; Wu, H.; Zhang, X.; Chen, S.; Xie, M.; Wu, F.; Lu, J.; Amine, K. Design of Surface Protective Layer of LiF/ FeF$_3$ Nanoparticles in Li-Rich Cathode for High-Capacity Li-Ion Batteries. *Nano Energy* **2015**, *15*, 164−176.

(49) Li, B.; Cheng, Z.; Zhang, N.; Sun, K. Self-Supported, Binder-Free 3D Hierarchical Iron Fluoride Flower-Like Array as High Power Cathode Material for Lithium Batteries. *Nano Energy* **2014**, *4*, 7−13.

(50) Li, C.; Mu, X.; van Aken, P. A.; Maier, J. A High-Capacity Cathode for Lithium Batteries Consisting of Porous Microspheres of Highly Amorphized Iron Fluoride Densified from Its Open Parent Phase. *Adv. Energy Mater.* **2013**, *3*, 113−119.

(51) Lee, J.; Sohn, K.; Hyeon, T. Low-Cost and Facile Synthesis of Mesocellular Carbon Foams. *Chem. Commun.* **2002**, 2674−2675.

(52) Lee, J.; Sohn, K.; Hyeon, T. Fabrication of Novel Mesocellular Carbon Foams with Uniform Ultralarge Mesopores. *J. Am. Chem. Soc.* **2001**, *123*, 5146−5147.

(53) Kang, E.; Jung, Y. S.; Cavanagh, A. S.; Kim, G. H.; George, S. M.; Dillon, A. C.; Kim, J. K.; Lee, J. Fe$_3$O$_4$ Nanoparticles Confined in Mesocellular Carbon Foam for High Performance Anode Materials for Lithium-Ion Batteries. *Adv. Funct. Mater.* **2011**, *21*, 2430−2438.

(54) Kim, S. W.; Seo, D. H.; Gwon, H.; Kim, J.; Kang, K. Fabrication of FeF$_3$ Nanoflowers on CNT Branches and Their Application to High Power Lithium Rechargeable Batteries. *Adv. Mater.* **2010**, *22*, 5260−5264.

(55) Liu, J.; Liu, W.; Ji, S.; Wan, Y.; Gu, M.; Yin, H.; Zhou, Y. Iron Fluoride Hollow Porous Microspheres: Facile Solution-Phase Synthesis and Their Application for Li-Ion Battery Cathodes. *Chem. - Eur. J.* **2014**, *20*, 5815−5820.

(56) Shen, Y.; Wang, X.; Hu, H.; Jiang, M.; Yang, X.; Shu, H. A Graphene Loading Heterogeneous Hydrated Forms Iron Based Fluoride Nanocomposite as Novel and High-Capacity Cathode Material for Lithium/Sodium Ion Batteries. *J. Power Sources* **2015**, *283*, 204−210.

(57) Wang, Z.; Luan, D.; Madhavi, S.; Hu, Y.; Lou, X. W. D. Assembling Carbon-Coated α-Fe$_2$O$_3$ Hollow Nanohorns on the CNT Backbone for Superior Lithium Storage Capability. *Energy Environ. Sci.* **2012**, *5*, 5252−5256.

(58) Luo, J.; Liu, J.; Zeng, Z.; Ng, C. F.; Ma, L.; Zhang, H.; Lin, J.; Shen, Z.; Fan, H. J. Three-Dimensional Graphene Foam Supported Fe$_3$O$_4$ Lithium Battery Anodes with Long Cycle Life and High Rate Capability. *Nano Lett.* **2013**, *13*, 6136−6143.

(59) Huang, X.; Chen, J.; Lu, Z.; Yu, H.; Yan, Q.; Hng, H. H. Carbon Inverse Opal Entrapped with Electrode Active Nanoparticles as High-Performance Anode for Lithium-Ion Batteries. *Sci. Rep.* **2013**, *3*, 2317.

(60) Li, L.; Jacobs, R.; Gao, P.; Gan, L.; Wang, F.; Morgan, D.; Jin, S. Origins of Large Voltage Hysteresis in High-Energy-Density Metal Fluoride Lithium-Ion Battery Conversion Electrodes. *J. Am. Chem. Soc.* **2016**, *138*, 2838−2848.

(61) Fan, X.; Luo, C.; Lamb, J.; Zhu, Y.; Xu, K.; Wang, C. PEDOT Encapsulated FeOF Nanorod Cathodes for High Energy Lithium-Ion Batteries. *Nano Lett.* **2015**, *15*, 7650−7656.

(62) Fan, X.; Zhu, Y.; Luo, C.; Gao, T.; Suo, L.; Liou, S.-C.; Xu, K.; Wang, C. In Situ Lithiated FeF$_3$/C Nanocomposite as High Energy Conversion-Reaction Cathode for Lithium-Ion Batteries. *J. Power Sources* **2016**, *307*, 435−442.

(63) Fan, X.; Zhu, Y.; Luo, C.; Suo, L.; Lin, Y.; Gao, T.; Xu, K.; Wang, C. Pomegranate-Structured Conversion-Reaction Cathode with

a Built-In Li Source for High Energy Li-Ion Batteries. *ACS Nano* **2016**, *10*, 5567−5577.

(64) Sohn, H.; Gordin, M. L.; Xu, T.; Chen, S.; Lv, D.; Song, J.; Manivannan, A.; Wang, D. Porous Spherical Carbon/Sulfur Nano-composites by Aerosol-Assisted Synthesis: The Effect of Pore Structure and Morphology on Their Electrochemical Performance As Lithium/Sulfur Battery Cathodes. *ACS Appl. Mater. Interfaces* **2014**, *6*, 7596−7606.

(65) Shen, L.; Zhang, X.; Uchaker, E.; Yuan, C.; Cao, G. Li$_4$Ti$_5$O$_{12}$ Nanoparticles Embedded in a Mesoporous Carbon Matrix as a Superior Anode Material for High Rate Lithium Ion Batteries. *Adv. Energy Mater.* **2012**, *2*, 691−698.

(66) Hyder, M. N.; Kavian, R.; Sultana, Z.; Saetia, K.; Chen, P.-Y.; Lee, S. W.; Shao-Horn, Y.; Hammond, P. T. Vacuum-Assisted Layer-by-Layer Nanocomposites for Self-Standing 3D Mesoporous Electro-des. *Chem. Mater.* **2014**, *26*, 5310−5318.

(67) Jiang, J.; Li, Y.; Liu, J.; Huang, X.; Yuan, C.; Lou, X. W. D. Recent Advances in Metal Oxide-Based Electrode Architecture Design for Electrochemical Energy Storage. *Adv. Mater.* **2012**, *24*, 5166−5180.

(68) Weng, W.; Pol, V. G.; Amine, K. Ultrasound Assisted Design of Sulfur/Carbon Cathodes with Partially Fluorinated Ether Electrolytes for Highly Efficient Li/S Batteries. *Adv. Mater.* **2013**, *25*, 1608−1615.

(69) Song, J.; Gordin, M. L.; Xu, T.; Chen, S.; Yu, Z.; Sohn, H.; Lu, J.; Ren, Y.; Duan, Y.; Wang, D. Strong Lithium Polysulfide Chemisorption on Electroactive Sites of Nitrogen-Doped Carbon Composites For High-Performance Lithium-Sulfur Battery Cathodes. *Angew. Chem., Int. Ed.* **2015**, *54*, 4325−4329; *Angew. Chem.* **2015**, *127*, 4399−4403.

(70) Lee, S.; Cho, Y.; Song, H. K.; Lee, K. T.; Cho, J. Carbon-Coated Single-Crystal LiMn$_2$O$_4$ Nanoparticle Clusters as Cathode Material for High-Energy and High-Power Lithium-Ion Batteries. *Angew. Chem., Int. Ed.* **2012**, *51*, 8748−8752; *Angew. Chem.* **2012**, *124*, 8878−8882.

(71) Zhang, C.; Wu, H. B.; Yuan, C.; Guo, Z.; Lou, X. W. D. Confining Sulfur in Double-Shelled Hollow Carbon Spheres for Lithium-Sulfur Batteries. *Angew. Chem., Int. Ed.* **2012**, *51*, 9592−9595; *Angew. Chem.* **2012**, *124*, 9730−9733.

(72) Xu, X.; Yan, M.; Tian, X.; Yang, C.; Shi, M.; Wei, Q.; Xu, L.; Mai, L. In Situ Investigation of Li and Na Ion Transport with Single Nanowire Electrochemical Devices. *Nano Lett.* **2015**, *15*, 3879−3884.

(73) Chun, J.; Chung, M.; Lee, J.; Kim, Y. Using Waste Li Ion Batteries as Cathodes in Rechargeable Li−Liquid Batteries. *Phys. Chem. Chem. Phys.* **2013**, *15*, 7036−7040.